



HAL
open science

Cosmological evolution of the Nitrogen abundance

Elisabeth Vangioni, Irina Dvorkin, Keith A. Olive, Yohan Dubois, Paolo Molaro, Patrick Petitjean, Joe Silk, Taysun Kimm

► **To cite this version:**

Elisabeth Vangioni, Irina Dvorkin, Keith A. Olive, Yohan Dubois, Paolo Molaro, et al.. Cosmological evolution of the Nitrogen abundance. *Monthly Notices of the Royal Astronomical Society*, 2018, 477 (1), pp.56-66. 10.1093/mnras/sty559 . hal-01856978

HAL Id: hal-01856978

<https://hal.science/hal-01856978>

Submitted on 4 Jun 2024

HAL is a multi-disciplinary open access archive for the deposit and dissemination of scientific research documents, whether they are published or not. The documents may come from teaching and research institutions in France or abroad, or from public or private research centers.

L'archive ouverte pluridisciplinaire **HAL**, est destinée au dépôt et à la diffusion de documents scientifiques de niveau recherche, publiés ou non, émanant des établissements d'enseignement et de recherche français ou étrangers, des laboratoires publics ou privés.

Cosmological evolution of the nitrogen abundance

Elisabeth Vangioni,^{1★} Irina Dvorkin,^{1,6★} Keith A. Olive,² Yohan Dubois,^{1★}
Paolo Molaro,³ Patrick Petitjean,¹ Joe Silk^{1,4} and Taysun Kimm⁵

¹*Sorbonne Universités, UPMC Univ Paris 6 et CNRS, UMR 7095, Institut d’Astrophysique de Paris, 98 bis bd Arago, F-75014 Paris, France*

²*William I. Fine Theoretical Physics Institute, University of Minnesota, Minneapolis, MN 55455, USA*

³*INAF Osservatorio Astronomico di Trieste, Via G.B. Tiepolo 11, I-34143 Trieste, Italy*

⁴*Department of Physics and Astronomy, The Johns Hopkins University, Baltimore, MD 21218, USA*

⁵*Department of Astronomy, Yonsei University, 50 Yonsei-ro, Seodaemun-gu, Seoul 03722, Republic of Korea*

⁶*Max Planck Institute for Gravitational Physics (Albert Einstein Institute), Am Mühlenberg 1, Postdam-golm D-14476, Germany*

Accepted 2018 February 19. Received 2018 February 19; in original form 2017 November 7

ABSTRACT

The abundance of nitrogen in the interstellar medium is a powerful probe of star formation processes over cosmological time-scales. Since nitrogen can be produced both in massive and intermediate-mass stars with metallicity-dependent yields, its evolution is challenging to model, as evidenced by the differences between theoretical predictions and observations. In this work, we attempt to identify the sources of these discrepancies using a cosmic evolution model. To further complicate matters, there is considerable dispersion in the abundances from observations of damped Ly α absorbers (DLAs) at $z \sim 2-3$. We study the evolution of nitrogen with a detailed cosmic chemical evolution model and find good agreement with these observations, including the relative abundances of (N/O) and (N/Si). We find that the principal contribution of nitrogen comes from intermediate-mass stars, with the exception of systems with the lowest N/H, where nitrogen production might possibly be dominated by massive stars. This last result could be strengthened if stellar rotation which is important at low metallicity can produce significant amounts of nitrogen. Moreover, these systems likely reside in host galaxies with stellar masses below $10^{8.5} M_{\odot}$. We also study the origin of the observed dispersion in nitrogen abundances using the cosmological hydrodynamical simulations Horizon-AGN. We conclude that this dispersion can originate from two effects: difference in the masses of the DLA host galaxies, and difference in their position inside the galaxy.

Key words: nuclear reactions, nucleosynthesis, abundances – ISM: abundances-galaxies: abundances – galaxies: ISM – large-scale structure of Universe.

1 INTRODUCTION

Measurements of chemical abundances in the interstellar medium (ISM) are a powerful probe of galaxy evolution and star formation processes. The total metallicity content, dominated by oxygen, reflects the star formation history, as well as the history of gas accretion and galactic outflows. To understand cosmic chemical evolution, theoretical models have been developed (e.g. Daigne et al. 2006; Davé, Finlator & Oppenheimer 2012; Lilly et al. 2013; Lu, Blanc & Benson 2015; Belfiore, Maiolino & Bothwell 2016) and studies of metal abundances in different galactic environments have unveiled important physical processes, such as galactic outflows (e.g. Belfiore et al. 2016) and the origin of star formation quenching (Peng, Maiolino & Cochrane 2015). These are based on galactic

chemical evolution models (Tinsley 1972; Pagel & Patchett 1975; Tinsley & Larson 1978; Matteucci 2004; Kobayashi et al. 2006) that now follow the cosmological evolution of the abundances as a function of redshift.

Observations of individual element abundances, as well as their relative abundances, are particularly informative, as they can constrain the nucleosynthetic processes as well as specific mass ranges of stars responsible for their production. Nitrogen is a particularly interesting (and challenging) element in this regard since it can be produced in both massive and intermediate-mass stars, which release it into the ISM on different time-scales. Thus, the study of the nitrogen abundance in the ISM, and in particular its relative abundance with respect to oxygen, which is produced mostly by massive, short-lived stars, poses interesting challenges for chemical evolution models.

Nitrogen can be produced as a *primary* element, in a sequence of nuclear reactions that involve only hydrogen and helium present

* E-mail: vangioni@iap.fr (EV); dvorkin@iap.fr (ID); dubois@iap.fr (YD)

in the star. In this case, its abundance grows in proportion to that of oxygen and (N/O) remains constant as (O/H) grows (Talbot & Arnett 1974), assuming metallicity-independent yields. Additionally, secondary nitrogen is produced from CNO elements present in the star, so that the nitrogen yield is metallicity-dependent and (N/O) is no longer constant (Clayton 1983; Arnett 1996). Interestingly, the observed (N/O) abundance exhibits a low-metallicity plateau, which is present in damped Ly α absorbers (DLAs) (Centuri3n et al. 2003; Molaro 2003) and is now evident in extragalactic H II regions with SDSS data (see Vincenzo et al. 2016, and references therein), which suggest primary nitrogen production. However, observations of the nitrogen abundance in DLAs (Pettini, Lipman & Hunstead 1995; Molaro et al. 1996; Lu, Sargent & Barlow 1998; Pettini et al. 2002; Centuri3n et al. 2003; Petitjean, Ledoux & Srianand 2008; Cooke et al. 2011; Zafar et al. 2014) have revealed a significant dispersion in (N/H) at any given redshift which adds another layer of difficulty. Thus, there is some uncertainty in the main production sites of nitrogen (massive or intermediate-mass stars), and it is still unclear which of these sites, if any, produces primary nitrogen in significant amounts. Indeed, in Centuri3n et al. (2003) it was concluded that DLAs do show evidence of primary N production at low metallicities and in addition that there are two plateaus. The $[N/\alpha]$ ratios are distributed in two groups: about 75 per cent of the DLAs show a mean value of $[N/\alpha] = -0.87$ and about 25 per cent show ratios at $[N/\alpha] = -1.45$. The lower group may originate from massive stars due to the tight linear correlation between N/H and α elements. The group with higher $[N/\alpha]$ provides evidence for primary production of intermediate-mass stars. The transition between the low- and high-N DLAs could result from the different lifetimes of massive and intermediate-mass stars.

The nitrogen abundance in the ISM was extensively studied in the context of galaxy evolution models (e.g. Pilyugin 1993; Fields & Olive 1998; Pilyugin 1999; Henry, Edmunds & K3ppen 2000; Tissera et al. 2002; Chiappini, Romano & Matteucci 2003; Pilyugin, Thuan & V3lchez 2003; Chiappini, Matteucci & Ballero 2005; Gavil3n, Moll3 & Buell 2006; Moll3 et al. 2006; Wu & Zhang 2013; Vincenzo et al. 2016). It should be noted that there is an inherent uncertainty in chemical evolution models as stemming from the uncertainty in stellar nitrogen abundances. Nevertheless, these studies confirmed that while the origin of the nitrogen abundance is a mix of primary and secondary sources, the total nitrogen budget is dominated by intermediate-mass stars in star-forming galaxies (as well as in other systems including DLAs) except perhaps at low metallicities. We note that various theoretical models typically utilize different sets of chemical yields, making the comparison of results problematic.

The goal of the current study is to examine the uncertainties in different stellar evolution models and their effect on the predicted cosmic evolution of the nitrogen abundance, specifically regarding DLAs observations. We use a uniform cosmic chemical evolution framework. We also compare the results of our semi-analytic model with the output of cosmological hydrodynamical simulations.

The paper is organized as follows. The data used for model comparison is described in Section 2 and we review the production of nitrogen and oxygen in several stellar evolution models in Section 3. In particular, we discuss the dependence of nitrogen and oxygen yields on stellar mass, metallicity, and rotation velocity. In Section 4.1, we show how these yields are implemented in our cosmic chemical evolution model and we describe the Horizon-AGN simulations in Section 4.2. Our results for the mean evolution of nitrogen and oxygen abundances in the ISM as a function of redshift are given in Section 5.1. In Section 5.2, we discuss the dispersion

in nitrogen abundances in DLAs in hydrodynamical cosmological Horizon-AGN simulations (Dubois et al. 2014) of galaxies of different masses and at different redshifts. We conclude and discuss future prospects in Section 6.

2 DATA

Nitrogen has been observed in various galactic environments and at different redshifts. Here, we summarize the observations used in this study (see for example Fig. 5).

Nitrogen is accurately measured in the H II regions of dwarf irregular and blue compact dwarf galaxies. We collect here the observations of van Zee et al. (1998) and van Zee & Haynes (2006) and of Izotov & Thuan (2004), James et al. (2015), Berg et al. (2012), and Izotov, Thuan & Guseva (2012), respectively. The flat slope in the (N/O) versus (O/H) plane found in star-forming dwarf galaxies below $12 + \log(O/H) = 7.7$ led to the conclusion that primary nitrogen has to be produced in massive stars, which promptly release it into the ISM (Thuan, Izotov & Lipovetsky 1995; Berg et al. 2012; Vincenzo et al. 2016). However, at low metallicity, intermediate-mass stars are also expected to produce nitrogen and as we will see, our detailed stellar evolution models do not generically predict sufficient primary nitrogen from massive stars to match the bulk of the observations.

Nitrogen can be also accurately measured in the DLAs which probe lower metallicities and high redshifts. We use here the compilation of high-redshift data coming from Zafar et al. (2014) and references therein. The nitrogen measurement compilation includes a sample of 108 systems but actual measurements of N and O, S, Si abundances are for 27 DLAs and sub-DLAs, of which 18 are critically drawn from the literature. The typical error bar of $[N/\alpha]$ in DLAs is of the order of 0.02 dex. This extended sample shows the $[N/\alpha]$ bimodal behaviour suggested in previous studies (see Centuri3n et al. 2003). Note that the high- $[N/\alpha]$ plateau in the DLAs is consistent with the low-metallicity tail of H II regions of dwarf irregular and blue compact dwarf galaxies but it extends to lower metallicities. Indeed, it is remarkable that observations in these very different environments and different redshifts establish a continuous relation in the N - α plane (although there is significant scatter; see Fig. 5). On the other hand, the low- $[N/\alpha]$ plateau (the lowest ever observed in any astrophysical site) gathered in Zafar et al. (2014) suggests the presence of a floor in $[N/\alpha]$ abundances, which may indicate a primary nitrogen production from fast rotating, massive stars in young or unevolved systems.

Unfortunately, N measurements in galactic halo stars are quite uncertain.

Historically, first measurements of N in metal poor stars were based on the NH 3360 band and provided almost solar abundances. For instance, $[N/Fe]$ were found -0.5 and -0.2 in the well-known halo stars HD 140283 and HD 64090, a result which was interpreted as a primary origin of N, and as a product of massive stars (Tomkin & Lambert 1984; Matteucci 1986).

Cayrel et al. (2004) and Spite et al. (2005) provided measurements based on the CN 3880 and NH 3360 bands, respectively. Spite et al. (2005) used the C/N abundance to separate the stars with mixed products from the CN cycle. There is a systematic offset for the abundances based on the two bands with the NH abundances being of 0.4 dex higher. When NH abundances are rescaled to match CN abundances, the unmixed stars with $[Fe/H] < -3.4$ show $[N/O] \approx -0.9$ overlapping the DLA's values though with significant scatter (cf. fig. 17 in Spite et al. 2005). Spite et al. (2005) note that accurate values of g_f and dissociation energy for NH as well as studies of

3D model atmosphere effects on the band strength are needed to assess the accuracy of the N abundances and therefore the stellar determinations will not be used in this paper.

Other observations of N abundances in nearby galaxies such as M33 and NGC 55 (Magrini, Corbelli & Galli 2007; Magrini, Gonçalves & Vajgel 2017) have abundances consistent with those used here. Recent surveys such as SDSS DR12 using 100 000 star-forming galaxies (Masters, Faisst & Capak 2016) or SDSS IV MaNGA using 550 nearby galaxies (Belfiore et al. 2017) show an interesting correlation between the N/O ratio and the stellar mass of these galaxies which could be more fundamental than the relation N/O versus O/H at a redshift around 0. Finally, note that N abundances have been measured in planetary nebulae and these studies can be used to test AGB stellar models (Stanghellini et al. 2006; Stanghellini & Haywood 2010; Cavichia et al. 2017; Ventura et al. 2017) at different metallicities/masses.

3 STELLAR NUCLEOSYNTHESIS OF NITROGEN

While there are many uncertainties regarding nitrogen yields in stars of different masses, the nuclear reactions leading to its formation are fairly well understood. Nitrogen is mainly produced in the CN branch of the CNO cycle (Clayton 1983; Arnett 1996) via the following chain of reactions: $^{12}\text{C}(p, \gamma)^{13}\text{N}(\beta^+, \nu)^{13}\text{C}(p, \gamma)^{14}\text{N}$ (note that nitrogen can also be produced in the ON cycle by transformation of ^{16}O , but at a much slower rate). The reaction $^{14}\text{N}(p, \gamma)^{15}\text{O}$ which depletes nitrogen has a relatively low cross-section enabling ^{14}N to accumulate with time. In this formation scenario nitrogen is a secondary element, whose production rate depends on the abundance of the CNO elements initially present in the star.

Alternatively, nitrogen can be produced as a primary element (Talbot & Arnett 1974). In this case, the reactions are the same as above, but the sequence of events is different: first, some ^{12}C is synthesized by the 3α reaction in a helium-burning region, and then this new ^{12}C is transported to the hydrogen-burning region, where the CNO cycle converts it to nitrogen. Thus, primary nitrogen is likely to be formed in stars with a helium-burning core and a CNO-burning shell, provided there is some mechanism that transports carbon between the two regions.

Observationally, the nucleosynthetic origin of nitrogen can be deduced by comparing its abundance to that of other elements. The abundance of primary nitrogen is proportional to that of the other primary elements (assuming metallicity-independent yields), while if nitrogen is produced as a secondary element, the increase in its abundance is proportional to the initial CNO content. Overall, the abundance of secondary nitrogen is proportional to the square of the CNO content. Note, however, that the evolution of nitrogen abundance in the ISM of a given galaxy is more complex, as it depends on the chemical evolution history of the galaxy and the inflow of primordial gas that dilutes the ISM.

Furthermore, various stellar evolution models predict different nitrogen yields, in particular, primary N yields from massive stars depend on Z and as a result might not produce a plateau. That is, if the yield of N/O is a function of metallicity, the resulting evolution of N/O versus O/H may not be constant and a plateau is not reproduced, thus confusing the interpretation of primary versus secondary origin of N. This adds an additional complication to the analysis.

The yields have been tested in a variety of chemical evolution models (Chiappini et al. 2006; Mollá et al. 2006; Romano

et al. 2010; Kobayashi, Karakas & Umeda 2011). These studies focused on reproducing the Milky Way chemical abundances which are used to calibrate different models. We next summarize several sets of nucleosynthetic yields used in this work for comparison.

3.1 Massive stars

In order to estimate the theoretical uncertainties in nitrogen yields in massive stars, we consider three different stellar evolution models: Woosley & Weaver (1995, WW95), Chieffi & Limongi (2004), and Nomoto et al. (2006). Specifically, WW95 present the evolution of massive stars at five different metallicities ($Z/Z_{\odot} = 0, 10^{-4}, 10^{-2}, 0.1, 1$) and masses from 11 to $40 M_{\odot}$. Chieffi & Limongi (2004) produce another set of explosive yields for masses in the range $13\text{--}35 M_{\odot}$ at six different metallicities ($Z = 0, 10^{-6}, 10^{-4}, 10^{-3}, 6 \times 10^{-3}, 0.02$). Nomoto et al. (2006) also study the mass range $13\text{--}35 M_{\odot}$ for four different metallicities: $Z = 0, 10^{-3}, 0.004, 0.02$. For illustration, Table 2 compares typical yields produced by these models at three metallicities ($Z/Z_{\odot} = 0, 0.001, 1$) and two masses: $15 M_{\odot}, 30 M_{\odot}$ by interpolating the published yields. For higher masses, we extrapolate the published yields. As we will show below, given the power-law initial mass function (IMF) used in our models, our results are not sensitive to these extrapolated yields. There are significant differences between the models, especially at low metallicities. These discrepancies are the result of the different models for the microphysics of pre-supernova evolution (such as the treatment of the convective layers) and different reaction rates, for example $^{12}\text{C}(\alpha, \gamma)^{16}\text{O}$ (see the discussion in Chieffi & Limongi 2004). Additional yields can be found in Heger & Woosley (2010), Limongi & Chieffi (2012), and Limongi (2017). The uncertainties in stellar yield assumptions were also studied in Romano et al. (2010), Mollá et al. (2015), Côté et al. (2016b), Côté et al. (2016a), and Andrews et al. (2017).

3.2 Intermediate-mass stars

We consider two stellar evolution models that target the evolution of intermediate-mass stars: van den Hoek & Groenewegen (1997) and Karakas (2010). van den Hoek & Groenewegen (1997) present the evolution of stars at five different metallicities ($Z = 0.001, 0.004, 0.008, 0.02, 0.04$; note that the last value is supersolar) and masses in the range $0.8\text{--}8 M_{\odot}$. Karakas (2010) present another set of yields for masses in the range $1\text{--}6 M_{\odot}$ at four different metallicities ($Z = 0.0001, 0.004, 0.008, 0.02$). Note that a recent study (Fishlock et al. 2014) has presented yields at $Z = 0.001$ for the same mass range. Table 1 presents typical yields for three metallicities ($Z = 0.0001, 0.004, 0.02$) and two masses, $2 M_{\odot}$ and $7 M_{\odot}$. The results of these two models are similar (note that the largest differences are again at the low-metallicity end). As we will show in what follows, intermediate-mass stars play a dominant role in producing the nitrogen observed in the ISM, therefore we do not expect large uncertainties in the modelled total nitrogen abundance. Note however that, since the yields are metallicity-dependent, uncertainties in the total metallicity (mainly due to oxygen abundance) may affect also the result for nitrogen.

Note that iron and silicon yields coming from SNIa are included in our model (0.5 and $0.1 M_{\odot}$, respectively). Details can be found in Daigne et al. (2006).

Table 1. Typical nitrogen and oxygen yields of intermediate-mass stars as a function of stellar mass and initial metallicity in different stellar evolution models (masses are in solar mass units): VdH97: van den Hoek & Groenewegen (1997), Karakas10: Karakas (2010).

Metallicity	$10^{-4} Z_{\odot}$		$10^{-4} Z_{\odot}$		$4 \cdot 10^{-3} Z_{\odot}$		$4 \cdot 10^{-3} Z_{\odot}$		Z_{\odot}		Z_{\odot}	
	2		7		2		7		2		7	
Stellar Mass												
Element	N	O	N	O	N	O	N	O	N	O	N	O
VdH97	10^{-4}	$1.5 \cdot 10^{-3}$	0.024	0.0036	0.001	0.001	0.062	0.0005	0.0045	0.015	0.096	0.06
Karakas10	$7.8 \cdot 10^{-5}$	$5.8 \cdot 10^{-4}$	0.039	0.001	0.000685	0.00293	0.063	0.0044	0.003	0.013	0.049	0.047

Table 2. Typical nitrogen and oxygen yields of massive stars as a function of stellar mass and initial metallicity in different stellar evolution models (masses are in solar mass units): WW95: Woosley & Weaver (1995), Chieffi04: Chieffi & Limongi (2004), Nomoto06: Nomoto et al. (2006). Note that the models strongly disagree at $Z = 0$.

Metallicity	0		0		$10^{-3} Z_{\odot}$		$10^{-3} Z_{\odot}$		Z_{\odot}		Z_{\odot}	
	15		30		15		30		15		30	
Stellar Mass												
Element	N	O	N	O	N	O	N	O	N	O	N	O
WW95	$3.63 \cdot 10^{-6}$	0.4	$3.53 \cdot 10^{-3}$	4.35	$4.85 \cdot 10^{-3}$	0.555	$1.08 \cdot 10^{-2}$	4.42	0.054	0.68	0.104	4.88
Chieffi04	$2.95 \cdot 10^{-7}$	0.346	$6.95 \cdot 10^{-2}$	3.04	$2.99 \cdot 10^{-3}$	0.527	$5.63 \cdot 10^{-3}$	3.75	0.051	0.516	0.0857	3.89
Nomoto06	$1.86 \cdot 10^{-3}$	0.773	$1.64 \cdot 10^{-6}$	4.81	$3.58 \cdot 10^{-3}$	0.294	$6.19 \cdot 10^{-3}$	5.33	0.062	0.16	0.102	3.22

Table 3. Typical nitrogen and oxygen yields (in solar mass units) of rotating and non-rotating stars for different stellar masses (Meynet & Maeder 2002b). In all the models, the metallicity is taken to be $Z = 10^{-5}$ and the velocity of rotation $v = 300 \text{ km s}^{-1}$.

Stellar Mass	2		7		15		20	
	N	O	N	O	N	O	N	O
$v = 0$	$1.7 \cdot 10^{-6}$	$1.9 \cdot 10^{-5}$	$1.6 \cdot 10^{-5}$	$1.2 \cdot 10^{-3}$	$3.5 \cdot 10^{-5}$	0.19	$4.6 \cdot 10^{-5}$	0.56
$v = 300 \text{ km s}^{-1}$	$6.4 \cdot 10^{-4}$	$1.1 \cdot 10^{-3}$	$4.2 \cdot 10^{-3}$	$5.6 \cdot 10^{-3}$	$4 \cdot 10^{-4}$	0.39	$3.4 \cdot 10^{-4}$	0.99

3.3 Stellar rotation

Stellar rotation, particularly important at low metallicities, can strongly affect the nucleosynthetic yields (Meynet & Maeder 2002a,b; Meynet & Pettini 2004). In particular, Meynet & Maeder (2002a) found that rotating, low-metallicity ($Z = 10^{-5}$) stars naturally produce primary nitrogen as a consequence of enhanced mixing between the hydrogen-burning shell and the core. Table 3 compares the yields calculated by Meynet & Maeder (2002b) of rotating ($v = 300 \text{ km s}^{-1}$) and non-rotating stars of different masses ($2\text{--}20 M_{\odot}$) at $Z = 10^{-5}$. It can be seen that both nitrogen and oxygen are produced in larger amounts in rotating stars, the difference with the non-rotating case reaching two orders of magnitude. Note however that this finding cannot have a significant impact on the evolution of the total nitrogen abundance, most of which is taking place in higher metallicity environments. We will nevertheless explore the impact of this set of yields, were it to hold for the entire range of metallicities, below.

4 MODELS

4.1 Cosmic chemical evolution model

In order to describe the cosmic chemical evolution of the ISM, we use the model developed by Daigne et al. (2004, 2006), Rollinde et al. (2009), and Vangioni et al. (2015) as outlined in the following. The initial gas content of galaxies is taken to be equal to the cosmic mean $f_{\text{baryon}} = \Omega_{\text{b}}/\Omega_{\text{m}}$, where Ω_{b} and Ω_{m} are the densities of baryons and total dark matter, respectively, in units of the critical density of the Universe. The gas is assumed to be primordial and metal-free and the calculation begins at a redshift $z = 20$. The model then follows two gas reservoirs, the intergalactic matter (IGM) and the ISM. Matter flows from IGM to ISM as the galaxies form, where

baryons are assumed to follow dark matter. In Daigne et al. (2006), the mean baryon accretion rate in each region was taken to be proportional to the fraction of baryons in structures, f_{coll} , and can be expressed as

$$a_{\text{b}}(t) = \Omega_{\text{b}} \left(\frac{3H_0^2}{8\pi G} \right) \left(\frac{dt}{dz} \right)^{-1} \left| \frac{df_{\text{coll}}}{dz} \right|, \quad (1)$$

where $f_{\text{coll}}(z)$ is given by the hierarchical model of structure formation (Press & Schechter 1974),

$$f_{\text{coll}}(z) = \frac{\int_{M_{\text{min}}}^{\infty} dM M f_{\text{PS}}(M, z)}{\int_0^{\infty} dM M f_{\text{PS}}(M, z)}, \quad (2)$$

and we assume that the minimum mass of dark matter haloes for star-forming structures is $10^7 M_{\odot}$. Accreted matter is assumed to be primordial and metal-free. Once inside galaxies, baryons form stars with rate $\psi(t)$ which we calibrate to observations, as described below. We assume a Salpeter IMF, $\Phi(m)$, with a slope $x = 1.35$, for $m_{\text{inf}} \leq m \leq m_{\text{sup}}$ with $m_{\text{inf}} = 0.1 M_{\odot}$ and $m_{\text{sup}} = 100 M_{\odot}$. Baryons can flow from structures back to the IGM due to galactic winds or feedback from supernovae (SNe). To sum up, the evolution of the total baryonic mass in the IGM and ISM is given by

$$\frac{dM_{\text{IGM}}}{dt} = -a_{\text{b}}(t) + o(t) \quad (3)$$

and

$$\frac{dM_{\text{ISM}}}{dt} = -\psi(t) + e(t) + a_{\text{b}}(t) - o(t), \quad (4)$$

where $\psi(t)$ is the cosmic star formation rate (SFR), $e(t)$ is the rate at which stellar mass is returned to the ISM by mass loss or stellar deaths, and $o(t)$ is the baryon outflow rate from structures into the IGM, which is obtained by energy arguments assuming the conservation of a fraction of the energy released in SNII and assuming

outflows with escape velocities. The outflow rate is actually the sum of two separate outflows (Daigne et al. 2004), $o(t) = o_w(t) + o_{sn}(t)$. The first one, $o_w(t)$, is a global outflow powered by the stellar explosions (galactic wind) and is similar to that described in Scully et al. (1997). The second term, $o_{sn}(t)$, corresponds to the fraction α of stellar SN ejecta which is flushed directly out of the structures, resulting in metal-enhanced winds as first proposed by Vader (1986). Note also, $o_w(t)$ carries the chemical composition of the ISM, whereas $o_{sn}(t)$ has the chemical composition of the SNe. The outflow rate is always small compared to the baryon accretion rate and detailed expressions for $o(t)$ are given in Daigne et al. (2006).

In addition, we follow the chemical composition of the ISM and the IGM as a function of time as described in Daigne et al. (2004). In particular, we do not use the instantaneous recycling approximation but calculate the rate at which gas is returned to the ISM including the effect of stellar lifetimes and computing stellar yields for each element and for different stellar mass ranges. The lifetimes of intermediate-mass stars ($0.9 < M/M_\odot < 8$) are taken from Maeder & Meynet (1989) and from Schaerer (2002) for more massive stars. Further details on the chemical evolution model can be found in Daigne et al. (2004, 2006) and Vangioni et al. (2015).

In typical models of galactic chemical evolution, the SFR resides among the set of physical quantities, with assumed forms (e.g. a decaying exponential in time or proportional to the gas density) with parameters which are fitted by the observations of the chemical abundances. Flexibility in the SFR was also adopted in the early cosmic chemical evolution models in Daigne et al. (2004, 2006) where SFR parameters were also required to fit the observed SFR at high redshift. However, over the last decade, there have been significant improvements in the observations of the SFR out to high redshift, $z \sim 10$ and in fact, there is very little flexibility in the SFR out to $z \sim 3$. In Rollinde et al. (2009), a fixed SFR was used based on the Springel & Hernquist (2003) form

$$\psi(z) = v \frac{a \exp(b(z - z_m))}{a - b + b \exp(a(z - z_m))}, \quad (5)$$

with parameters fitted directly to the observed SFR. Here, we use the cosmic SFR modelled in Vangioni et al. (2015) with $v = 0.178 M_\odot \text{ yr}^{-1} \text{ Mpc}^{-3}$, $z_m = 2.00$, $a = 2.37$, and $b = 1.80$. Fig. 1 (upper panel) shows the SFR in our model (black line) and observations compiled by Behroozi, Wechsler & Conroy (2013), as well as high-redshift measurements by Bouwens et al. (2014) and Oesch et al. (2014). For a comparison, we also show the SFR from Madau & Dickinson (2014).

The SFR can also be constrained by using the optical depth to reionization, which depends on the rate of production of ionizing photons by massive stars. We calculate the optical depth to reionization τ as described in Vangioni et al. (2015), in particular we use the tables in Schaerer (2002) for the number of photons produced by massive stars and assume an escape fraction of $f_{esc} = 0.2$. The resulting optical depth is shown in Fig. 1 (bottom panel) and compared to the constraints obtained from measurements of the cosmic microwave background (Planck Collaboration XLVI et al. 2016a; Planck Collaboration XLVII et al. 2016b). Note that the SFR of Madau & Dickinson (2014) is flatter than the SFR used in our model and produces slightly higher rates than observed at $z \sim 10$. Consequently, the optical depth is also larger than that observed by Planck, unless f_{esc} is as low as 0.05. Note that there are other parameters which introduce additional uncertainties in the model prediction of the optical depth. Finally, we stress that this model does not follow galaxy properties individually but averaged properties of the ISM and of the IGM within a sub-volume of the Universe.

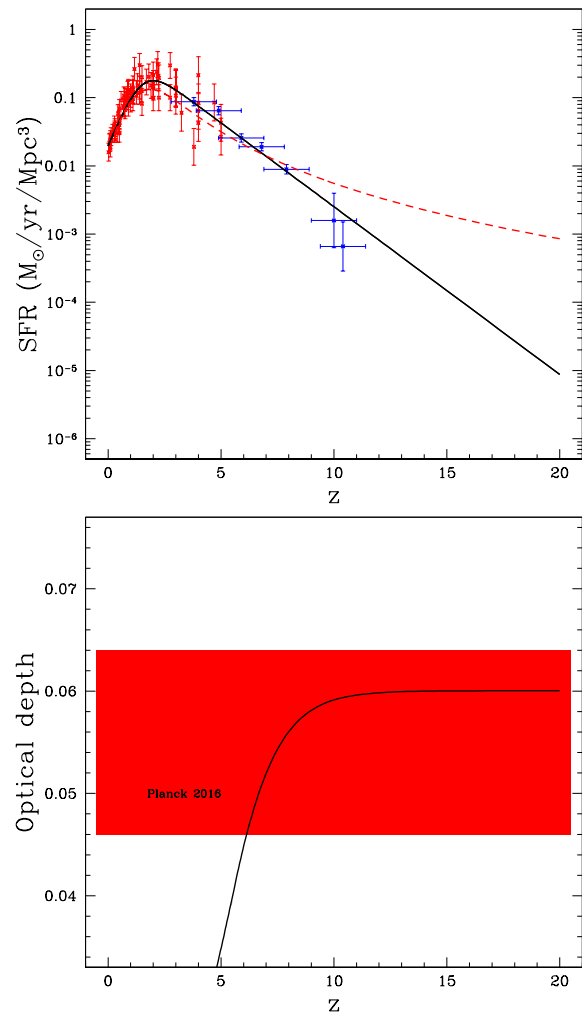


Figure 1. Upper panel: The SFR as a function of redshift used in our model (black line) compared to observations: Behroozi et al. (2013) (red points), Bouwens et al. (2014); Oesch et al. (2014) (blue points). The SFR in Madau & Dickinson (2014) is shown for a comparison (red dashed line). Lower panel: Evolution of the optical depth to reionization as a function of redshift. The observational constraint is indicated by a red horizontal strip (Planck Collaboration XLVI et al. 2016a; Planck Collaboration XLVII et al. 2016b).

As a result, metallicities generally remain subsolar. For further details on the evolution of the metallicity with redshift in the context of a merger-tree model, see Dvorkin et al. (2015, 2016). Note that in this model, we do not follow the chemical evolution of individual galaxies, but the averages over relatively large volumes, treating each region of the Universe as a closed box. We are currently working on an updated model where each galaxy is treated individually, as part of a larger project that also studies other chemical species, and will present this model in a forthcoming publication.

4.2 Horizon-AGN simulation

The details of the simulation can be found in Dubois et al. (2014) and references therein, but we recall here the main aspects of the simulation. The Horizon-AGN simulation is a hydrodynamical cosmological simulation of a flat Lambda Cold Dark Matter universe performed with the adaptive mesh refinement code RAMSES (Teyssier 2002) using a WMAP-7-like cosmology

(Komatsu et al. 2011) with $\Omega_m = 0.272$, $\Omega_\Lambda = 0.728$, $\sigma_8 = 0.81$, $\Omega_b = 0.045$, $H_0 = 70.4 \text{ km s}^{-1} \text{ Mpc}^{-1}$, and $n_s = 0.967$. The box size is $100 \text{ h}^{-1} \text{ Mpc}$ filled 1024^3 dark matter particles with a mass resolution of $8 \times 10^7 M_\odot$. The mesh refinement is triggered according to a quasi-Lagrangian criterion when the mass within a cell is eight times the dark matter mass resolution down to a spatial resolution of 1 kpc. The Horizon-AGN simulation includes metal-dependent gas cooling with ultraviolet background heating after reionization at $z = 10$, a Schmidt star formation law of a constant efficiency of 2 per cent, feedback from stars including stellar winds, type II and type Ia SNe assuming a Salpeter-like IMF (Kaviraj et al. 2017), and feedback from active galactic nuclei together with the self-consistent growth of black holes following an Eddington-limited Bondi–Hoyle–Littleton accretion rate.

The mass loss from stellar winds and SNe is modelled using `STARBURST99` (Vázquez & Leitherer 2005). Specifically, Horizon-AGN adopts the ‘Evolution’ model (Leitherer, Robert & Drissen 1992), which computes the outflow rates from stellar winds with the Padova tracks plus thermally pulsing AGB stars (Bertelli et al. 1994; Girardi et al. 2000). This model is based on the SN yields from Woosley & Weaver (1995) for massive stars with mass $8 \leq M/M_\odot \leq 40$. For low-mass to intermediate-mass ($0.1 \leq M/M_\odot \leq 7$) stars, the chemical yields are taken from the chemical abundance at the stellar surface computed from the Padova stellar tracks (Girardi et al. 2000). These yields are similar to those coming from Karakas (2010) and van den Hoek & Groenewegen (1997). Note that most (~ 80 per cent) of the nitrogen is produced before the age of 50 Myr via SNe, whereas intermediate-mass stars account for only 20 per cent, at that time. The yields for SN Type Ia are taken from Nomoto et al. (2006), but their contributions to the total production of nitrogen are negligible.

To extract the metal mass content of the galaxies, we include all gas cells within the effective radius of the galaxy and with a gas density above 0.1 H cm^{-3} , which is our gas density threshold for star formation.

5 RESULTS

5.1 Evolution of nitrogen abundance with redshift

In order to study the production of nitrogen and its abundance in the ISM, we implement the stellar evolution models discussed in Section 3 in our galaxy evolution model. We use the yields discussed in Sections 3.1 and 3.2 for stars in the mass ranges $8 < M/M_\odot < 40$ and $0.9 < M/M_\odot < 8.0$, respectively. An interpolation is made between different metallicities and masses, and tabulated values are extrapolated for masses above $40M_\odot$, which correspond to a small fraction of the population of massive stars (i.e. $(40^{-x} - 100^{-x}) / (8^{-x} - 100^{-x}) \simeq 8$ per cent). We adopt the solar abundances from Asplund et al. (2009). We stress the importance of including metallicity-dependent yields, rather than constant yields, as demonstrated in Fig. 2. In this figure, we compare the resulting ratio of $[N/O]$, assuming constant yields (blue curves) to a metallicity-dependent yield (red curve). In each case, we employ the yields from Nomoto et al. (2006). For constant yields, we show results for both solar (solid curve) and metal-free (dashed curve) yields. As one might expect from Table 2, the produced N/O ratio is significantly larger in solar metallicity stars than in metal-free stars. The model with metal-dependent yields interpolates between the two.

We now compare the results of our model to the observed abundance measurements, focusing on the comparison between different stellar evolution models and the contribution of massive versus

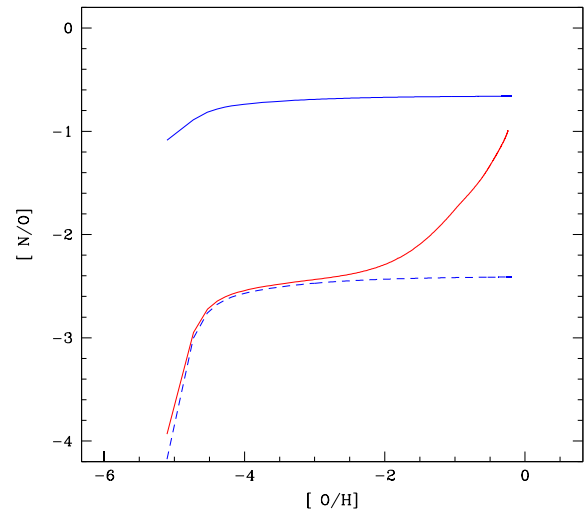


Figure 2. The evolution of nitrogen in the ISM (total) produced in massive stars in the semi-analytical model. Blue lines: corresponding to the constant yields from Nomoto et al. (2006) for $Z = Z_\odot$ and $Z = 0$ for solid and dashed lines, respectively. Red line: metallicity-dependent yields from Nomoto et al. (2006). Note that in the latter case $[N/O]$ increases sharply with metallicity, as can be anticipated from Table 2.

intermediate-mass stars to the nitrogen content of the ISM. Fig. 3 (upper panel) shows the evolution of nitrogen abundance in our model with different sets of yields: blue dotted and solid lines correspond to models that include both intermediate-mass stars (IMS) with yields taken from Karakas (2010) and van den Hoek & Groenewegen (1997), respectively, and massive stars, with yields taken from Nomoto et al. (2006). As can be anticipated from Table 2, the two sets of yields for intermediate-mass stars produce very similar results. Red solid, dashed, and dotted lines correspond to models that include only the contribution of massive stars, with the yields taken from Chieffi & Limongi (2004), Woosley & Weaver (1995), and Nomoto et al. (2006), respectively. In this case, the differences in nitrogen and oxygen yields shown in Table 2 are translated into a relatively large vertical offset between the red curves. It is clear, however, that intermediate-mass stars dominate the production of nitrogen at all redshifts and this contribution is needed to explain the abundances with the highest values of $[N/H]$. Note that the differences in the yields of massive stars do not affect the uncertainty in the total nitrogen budget. This result confirms the finding of Wu & Zhang (2013) for massive star-forming galaxies. We also note that the scatter in $[N/H]$ observed at any given redshift is much greater than the observational uncertainty. This scatter can originate from differences in structure formation histories of the different galaxies that host these DLAs, as we discuss below, including different accretion and star formation histories. In addition, the scatter, for now, masks any trend in the observations of $[N/H]$ with redshift as predicted by the models.

As in the upper panel of Fig. 3, Fig. 4 shows the evolution of the relative $[N/O]$ abundance in our model as a function of z , with different sets of yields. We note that massive stars (red curves, modulo uncertainties related to stellar yields) which form the first nitrogen atoms can reproduce the lowest part of DLA observations ($[N/O] = -1.5$). It is interesting to note that blue and red curves frame the bulk of observations possibly corresponding to a progressive increase in nitrogen coming from intermediate-mass stars.

The lower panel in Fig. 3 shows the effect of stellar rotation, where we used *constant* yields (computed for $Z = 10^{-5}$) taken from

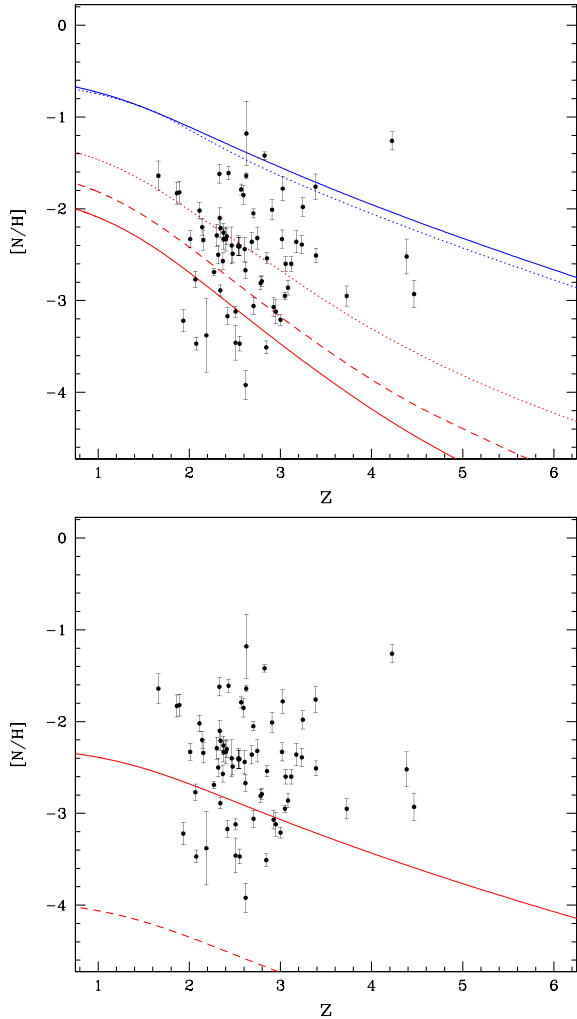


Figure 3. Evolution of nitrogen abundance with redshift for different stellar evolution models. Upper panel: Nitrogen produced in massive stars only, with yields taken from Chieffi & Limongi (2004), Woosley & Weaver (1995), and Nomoto et al. (2006) (red solid, dashed, and dotted lines, respectively) and the total nitrogen budget (blue lines). The yields for intermediate-mass stars are taken from Karakas (2010) and van den Hoek & Groenewegen (1997) for the dotted and solid blue lines, respectively, the yields for massive stars are taken from Nomoto et al. (2006) in both cases. Lower panel: The evolution of nitrogen abundance assuming all stars are rotating (solid) or non-rotating (dashed) and using constant yields, taken as the yields from Meynet & Maeder (2002b) at $Z = 10^{-5}$. Data taken from Zafar et al. (2014) and references therein (black points).

Meynet & Maeder (2002b). While, as evident also from Table 3, rotating low-metallicity stars produce significant amounts of primary nitrogen, this model is in fact not realistic since the actual metallicity at the relevant redshifts is much higher than 10^{-5} . Further studies of rotating stars including yield tables at higher metallicity are required in order to elucidate their role in the cosmic nitrogen enrichment.

Fig. 5 shows the nitrogen abundance as a function of metallicity in DLAs. The data have been detailed in Section 2. As one can see, the data are well reproduced by our model, shown by the blue lines. As shown previously, relatively little nitrogen is produced in massive stars (red lines). We also note that when available, we plot data using oxygen abundances. However, in some cases, either Si or S is used as a surrogate for the metallicity. The curves, nevertheless,

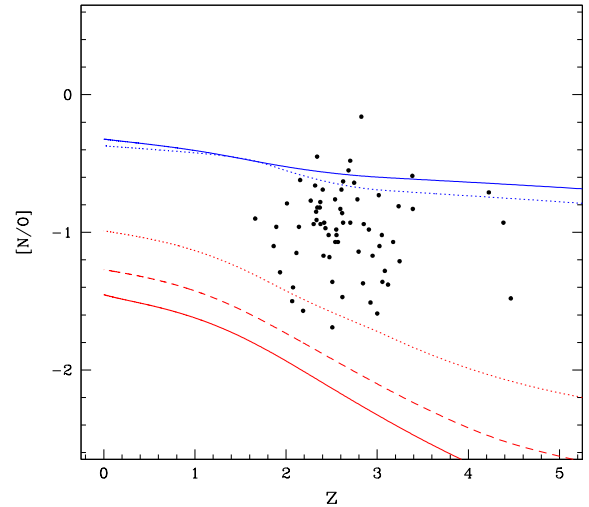


Figure 4. As in Fig. 3, the relative abundance $[N/O]$ as a function of redshift.

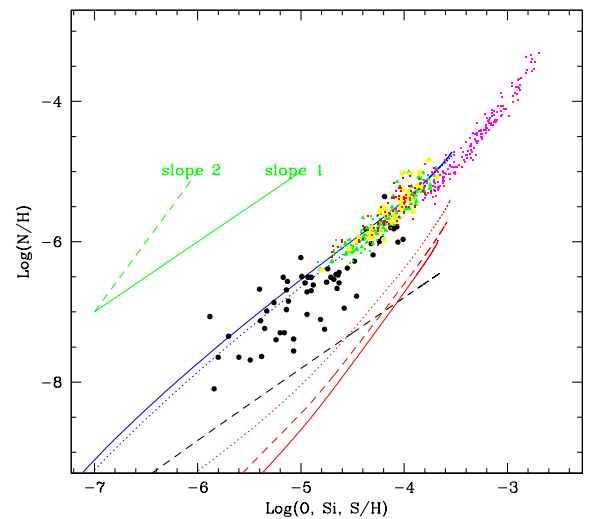


Figure 5. The nitrogen abundance as a function of metallicity in our model with different sets of yields (line notation as in Fig. 3) compared to observations in DLAs Zafar et al. (2014) (black points), H II regions of spiral galaxies (magenta points; van Zee et al. 1998; van Zee & Haynes 2006) and blue compact dwarf galaxies (green, blue, and yellow points, respectively; Izotov & Thuan 2004; Berg et al. 2012; Izotov et al. 2012; James et al. 2015). Dashed black line corresponds to the case of rotating stars, with constant yields (at $Z = 10^{-5}$) taken from Meynet & Maeder (2002b).

show the evolution of N/H versus O/H as predicted by the model. The deficiency in a uniform data set introduces additional uncertainty and scatter when comparing with O/H . As noted above, our abundances represent a mean value which remain subsolar, and thus we cannot expect to reproduce the abundances of $z = 0$ H II regions of spiral galaxies shown by the magenta points, in this context.

Fig. 6 shows the effect of our extrapolation of stellar yields above $40 M_{\odot}$. The blue solid curve is that shown in Fig. 5 where the yields above $40 M_{\odot}$ have been extrapolated. However, as remarked earlier, the fraction of stars in this mass range is rather limited and we are not very sensitive to this procedure. The blue dashed curve in Fig. 6 shows the calculated abundances when the yields above $40 M_{\odot}$ are held constant. As one can see, the effect is minimal.

It is interesting to note that our models with only massive stars (red curves) do not exhibit the characteristic slope of 1 associated

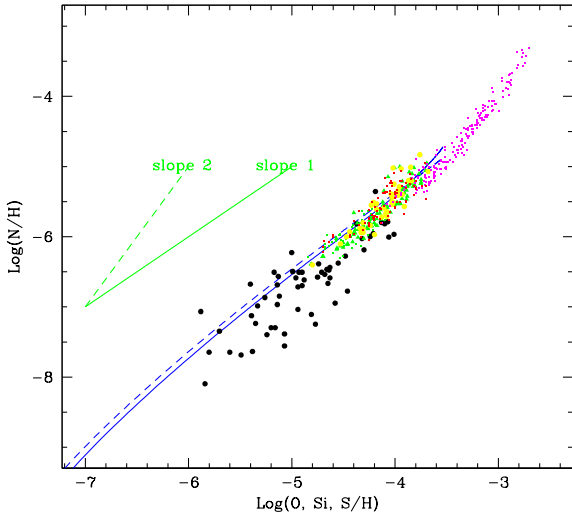


Figure 6. As in Fig. 5 showing a comparison of the model using the yields of Nomoto et al. (2006) and van den Hoek & Groenewegen (1997) when yields above $40 M_{\odot}$ have been extrapolated (solid) and when the yields are held constant above $40 M_{\odot}$.

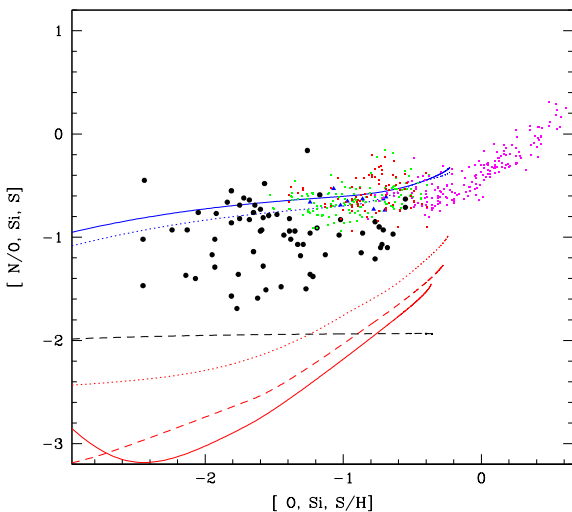


Figure 7. As in Fig. 5, the relative abundance $[N/O]$ as a function of metallicity.

with primary production. As we have stressed earlier, this is due to the metallicity-dependent yields used in the calculation. In contrast, as seen by the black dashed curve, when metallicity-independent yields are used, the slope is indeed found to be 1. One sees a slight steepening starting at a metallicity of roughly $\log(O/H) \sim -3.5$.

We further emphasize that due to the substantial dispersion in the data for O/H versus redshift (or more precisely α/H versus redshift), that a direct mapping of N/H versus z to N/H versus α/H is not possible. That is, since there is no one-to-one relation between α/H and redshift, points will shift relative to model predictions when comparing results in Figs 3 and 5.

Bearing this ambiguity in mind, the relative abundance of nitrogen and oxygen is further explored in Fig. 7 which also exhibits the scatter observed in DLAs (black points) and compact dwarf galaxies (green, blue, and yellow points). It can be seen that the ratio $[N/O]$ for nitrogen that originates in massive stars is well below the observational points. Thus, according to our model, the bulk of

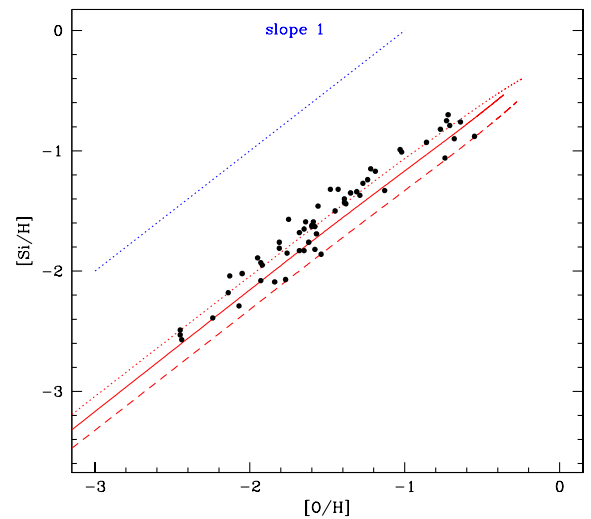
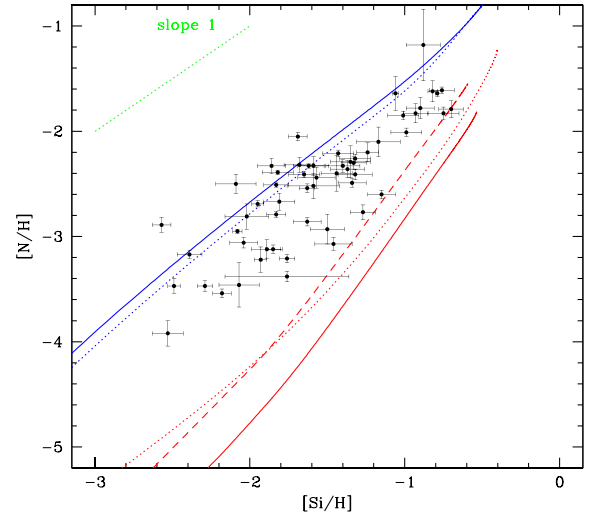


Figure 8. Upper panel: As in Fig. 3 showing the evolution of $[N/H]$ as a function of $[Si/H]$ in our model. Data is taken from the compilation of Zafar et al. (2014) (black points). Lower panel: The correlation between Si and O abundances.

the nitrogen observed in DLAs and dwarf galaxies originates from intermediate-mass stars. A similar conclusion was reached by Henry et al. (2000), who found the bulk of cosmic nitrogen to be formed in intermediate-mass stars as a primary source at low metallicity and secondary source at higher metallicity. We see once again that the model with rotating stars with constant yields is flat when plotting $[N/O]$ in contrast to the models with metallicity-dependent yields. Note that our models do not attain solar abundances (of either O/H or N/H) as the curves represent average abundances (throughout the universe) and are thus heavily weighted by low-mass objects with subsolar abundances.

Finally, we use our model to explore the relative abundances of nitrogen and other elements. The upper panel in Fig. 8 shows the tight correlation between $[N/H]$ and $[Si/H]$ (albeit with a considerable dispersion), reproduced by our model. Note that the observed correlation between $[Si/H]$ and $[O/H]$, shown in the lower panel of Fig. 8, is much tighter, since both O and Si are produced in massive stars and are simultaneously released into the ISM.

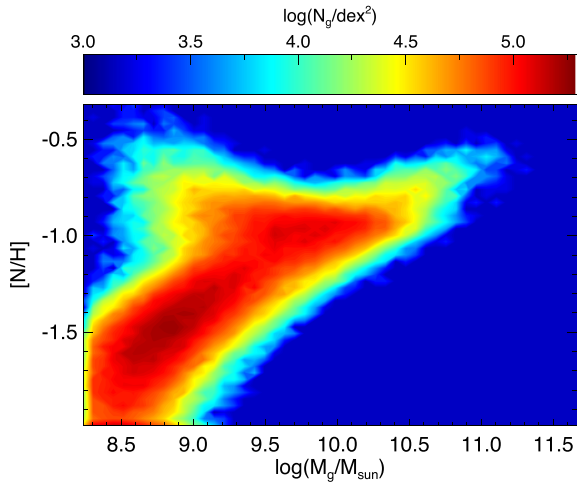


Figure 9. The nitrogen abundance in the cold gas of galaxies as a function of galaxy stellar mass in Horizon-AGN at $z = 2$. The shading corresponds to the relative number of galaxies in the sample in each abundance-mass bin.

5.2 Dispersion in nitrogen abundances

As can be seen in Figs 3 and 7, there is a significant dispersion in nitrogen abundance at any given redshift. Here, we study the dispersion due to the difference in the masses of DLA host galaxies.

The masses of the DLA host galaxies may vary across our sample, and while they are very difficult to measure, they are expected to affect the DLA properties. Indeed, a mass–metallicity relation, similar to that observed in galaxies in emission, might be present in DLAs (Neeleman et al. 2013). The semi-analytic models presented above are not suitable to study this issue since they do not resolve individual galaxies. In this section, we therefore use the outcome of the Horizon-AGN simulation (Dubois et al. 2014) described above to estimate the dispersion in nitrogen abundance in the ISM of $z \sim 2$ galaxies.

The result of the abundance of nitrogen in galaxies as a function of the galaxy stellar mass in Horizon-AGN at $z = 2$ is shown in Fig. 9. We notice first that there is very little dispersion at larger masses ($M > 10^{10.5} M_{\odot}$) with the amount of dispersion increasing at lower masses. Below $10^{8.5} M_{\odot}$, the amount of dispersion is approximately 1.5 dex and is slightly less what is observed. Note that the observations of the lowest DLA abundances of N/H can be well explained if their mass corresponds to a stellar mass of $10^{8.5} M_{\odot}$ or less.

Fig. 10 shows the nitrogen-to-oxygen ratio as a function of galaxy stellar mass at $z = 0$ in Horizon-AGN compared to the CALIFA data from Pérez-Montero et al. (2016). The amount of nitrogen relative to oxygen is on average lower in Horizon-AGN with respect to the data at any mass. Note that we have also tested the effect of AGN feedback on the amount of nitrogen in the cold gas in galaxies using the Horizon-noAGN simulation (Dubois et al. 2016; Peirani et al. 2017) and we found little difference with the simulation including AGN feedback, a result in agreement with recent simulations from Taylor & Kobayashi (2015).

Finally, we study the effect of differences in DLA position within the host galaxy. We draw several line of sights through our simulation box, one every 1 kpc in the x and y coordinates, and compute the nitrogen abundance in the cold ISM gas along each line of sight (at $z = 2$, there are $\sim 7 \times 10^6$ line of sights containing cold gas with nitrogen). We repeat this procedure for three different redshifts and compare the average and the standard deviation with data points

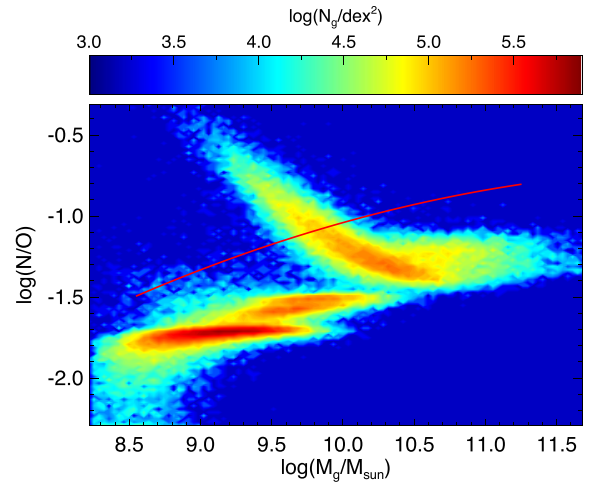


Figure 10. The nitrogen over oxygen ratio in the cold gas of galaxies as a function of galaxy stellar mass in Horizon-AGN at $z = 0$ compared with the CALIFA observations from Pérez-Montero et al. (2016) (red solid line). The shading corresponds to the number density of galaxies in the sample in each abundance-mass bin.

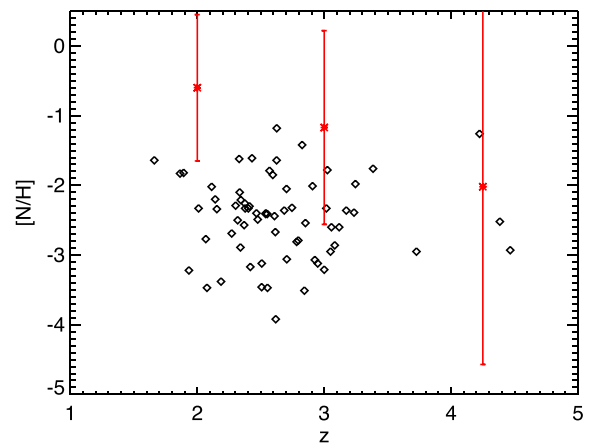


Figure 11. Nitrogen abundance as a function of redshift for data points from Zafar et al. (2014) (black diamonds) and for the Horizon-AGN simulation (red symbols with a 1σ standard deviation). The result of Horizon-AGN is obtained with the compilation of all possible line of sights passing through cold gas in galaxies at the three different plotted redshifts.

from Zafar et al. (2014). As can be seen in Fig. 11, the Horizon-AGN simulation predicts higher values of the nitrogen abundance at $z = 2$ and 3 compared with observations, but its value is comparable to the few data points at $z = 4$.

Finally, the dispersion of the nitrogen line of sight in Horizon-AGN is large ~ 1 dex at $z = 2$ and 3 and ~ 2 dex at $z = 4$, which is very close to the dispersion observed in the data points for the lowest redshift range.

This is the result of having a large variety of possible line of sights going through galaxies of various masses, that are different stages of their chemical evolution, as well as line of sight probing different regions within the same galaxy: either gas with an old population of stars in the centre of galaxies, or freshly accreted gas from the IGM forming young stars in the outskirts.

6 CONCLUSIONS

In this paper, we explored the evolution of the nitrogen abundance in the ISM and its dispersion using a cosmological galaxy evolution model. In particular, we explored several sets of nucleosynthetic yields currently used by various groups and showed that the bulk of nitrogen in the ISM is produced by intermediate-mass stars. At very low metallicity, nitrogen production can be explained by massive stars production while at higher metallicity nitrogen is essentially produced by the IMS.

Since the yields of this class of objects are consistent between models (contrary to the case of massive stars), it follows that the total nitrogen mass produced by a given stellar population can be calculated with a reasonably high accuracy.

Furthermore, we explored the sources of dispersion in the nitrogen abundance in DLAs using the Horizon-AGN hydrodynamical simulations and concluded that it can be caused by the difference in the masses of the host galaxies. In particular, we found that this dispersion grows with decreasing galaxy mass. Another source of dispersion is the difference in the lines of sights that corresponds to different DLAs. While these effects contribute to the observed dispersion, further work is needed in order to understand the relative contribution of each effect. In a forthcoming publication, we use an updated model where each galaxy will be treated individually (obtaining the evolution as a function of galaxy stellar mass), together with a larger project that also studies other chemical species.

ACKNOWLEDGEMENTS

We thank warmly Georges Meynet for very fruitful discussions. This work is made in the ILP LABEX (under reference ANR-10-LABX-63) supported by French state funds managed by the ANR within the Investissements d'Avenir programme under reference ANR-11-IDEX-0004-02. The work of KAO was supported in part by DOE grant DE-SC0011842 at the University of Minnesota. TK is supported by the National Research Foundation of Korea to the Center for Galaxy Evolution Research (No. 2017R1A5A1070354).

REFERENCES

- Andrews B. H., Weinberg D. H., Schönrich R., Johnson J. A., 2017, *ApJ*, 835, 224
- Arnett D., 1996, *Supernovae and Nucleosynthesis*. Princeton Univ. Press, Princeton
- Asplund M., Grevesse N., Sauval A. J., Scott P., 2009, *ARA&A*, 47, 481
- Behroozi P. S., Wechsler R. H., Conroy C., 2013, *ApJ*, 770, 57
- Belfiore F., Maiolino R., Bothwell M., 2016, *MNRAS*, 455, 1218
- Belfiore F. et al., 2017, *MNRAS*, 469, 151
- Berg D. A. et al., 2012, *ApJ*, 754, 98
- Bertelli G., Bressan A., Chiosi C., Fagotto F., Nasi E., 1994, *A&AS*, 106, 275
- Bouwens R. J. et al., 2014, *ApJ*, 795, 126
- Cavichia O., Costa R. D. D., Maciel W. J., Mollá M., 2017, *MNRAS*, 468, 272
- Cayrel R. et al., 2004, *A&A*, 416, 1117
- Centurión M., Molaro P., Vladilo G., Péroux C., Levshakov S. A., D'Odorico V., 2003, *A&A*, 403, 55
- Chiappini C., Romano D., Matteucci F., 2003, *MNRAS*, 339, 63
- Chiappini C., Matteucci F., Ballero S. K., 2005, *A&A*, 437, 429
- Chiappini C., Hirschi R., Meynet G., Ekström S., Maeder A., Matteucci F., 2006, *A&A*, 449, L27
- Chieffi A., Limongi M., 2004, *ApJ*, 608, 405
- Clayton D. D., 1983, *Principles of Stellar Evolution and Nucleosynthesis*. Chicago Univ. Press, Chicago
- Cooke R., Pettini M., Steidel C. C., Rudie G. C., Nissen P. E., 2011, *MNRAS*, 417, 1534
- Côté B., West C., Heger A., Ritter C., O'Shea B. W., Herwig F., Travaglio C., Bisterzo S., 2016a, *MNRAS*, 463, 3755
- Côté B., Ritter C., O'Shea B. W., Herwig F., Pignatari M., Jones S., Fryer C. L., 2016b, *ApJ*, 824, 82
- Daigne F., Olive K. A., Vangioni-Flam E., Silk J., Audouze J., 2004, *ApJ*, 617, 693
- Daigne F., Olive K. A., Silk J., Stoehr F., Vangioni E., 2006, *ApJ*, 647, 773
- Davé R., Finlator K., Oppenheimer B. D., 2012, *MNRAS*, 421, 98
- Dubois Y. et al., 2014, *MNRAS*, 444, 1453
- Dubois Y., Peirani S., Pichon C., Devriendt J., Gavazzi R., Welker C., Volonteri M., 2016, *MNRAS*, 463, 3948
- Dvorkin I., Silk J., Vangioni E., Petitjean P., Olive K. A., 2015, *MNRAS*, 452, L36
- Dvorkin I., Vangioni E., Silk J., Petitjean P., Olive K. A., 2016, *MNRAS*, 458, L104
- Fields B. D., Olive K. A., 1998, *ApJ*, 506, 177
- Fishlock C. K., Karakas A. I., Lugaro M., Yong D., 2014, *ApJ*, 797, 44
- Gavilán M., Mollá M., Buell J. F., 2006, *A&A*, 450, 509
- Girardi L., Bressan A., Bertelli G., Chiosi C., 2000, *A&AS*, 141, 371
- Heger A., Woosley S. E., 2010, *ApJ*, 724, 341
- Henry R. B. C., Edmunds M. G., Köppen J., 2000, *ApJ*, 541, 660
- Izotov Y. I., Thuan T. X., 2004, *ApJ*, 602, 200
- Izotov Y. I., Thuan T. X., Guseva N. G., 2012, *A&A*, 546, A122
- James B. L., Koposov S., Stark D. P., Belokurov V., Pettini M., Olszewski E. W., 2015, *MNRAS*, 448, 2687
- Karakas A. I., 2010, *MNRAS*, 403, 1413
- Kaviraj S. et al., 2017, *MNRAS*, 467, 4739
- Kobayashi C., Umeda H., Nomoto K., Tominaga N., Ohkubo T., 2006, *ApJ*, 653, 1145
- Kobayashi C., Karakas A. I., Umeda H., 2011, *MNRAS*, 414, 3231
- Komatsu E. et al., 2011, *ApJS*, 192, 18
- Leitherer C., Robert C., Drissen L., 1992, *ApJ*, 401, 596
- Lilly S. J., Carollo C. M., Pipino A., Renzini A., Peng Y., 2013, *ApJ*, 772, 119
- Limongi M., 2017, in Alsabti A., Murdin P., eds, *Handbook of Supernovae*. Springer
- Limongi M., Chieffi A., 2012, *ApJS*, 199, 38
- Lu L., Sargent W. L. W., Barlow T. A., 1998, *AJ*, 115, 55
- Lu Y., Blanc G. A., Benson A., 2015, *ApJ*, 808, 129
- Madau P., Dickinson M., 2014, *ARA&A*, 52, 415
- Maeder A., Meynet G., 1989, *A&A*, 210, 155
- Magrini L., Corbelli E., Galli D., 2007, *A&A*, 470, 843
- Magrini L., Gonçalves D. R., Vajgel B., 2017, *MNRAS*, 464, 739
- Masters D., Faisst A., Capak P., 2016, *ApJ*, 828, 18
- Matteucci F., 1986, *MNRAS*, 221, 911
- Matteucci F., 2004, in Mac Williams A., Rauch R., eds, *Origin and Evolution of the Elements*, Cambridge Univ. Press, p. 85
- Meynet G., Maeder A., 2002a, *A&A*, 381, L25
- Meynet G., Maeder A., 2002b, *A&A*, 390, 561
- Meynet G., Pettini M., 2004, in Maeder A., Eenens P., eds, *Proc. IAU Symp. 215, Stellar Rotation*. Kluwer, Dordrecht, p. 579
- Molaro P., 2003, *Elemental abundances in old stars and Damped Lyman Alpha systems*, 25th meeting of the IAU. p. 43
- Molaro P., D'Odorico S., Fontana A., Savaglio S., Vladilo G., 1996, *A&A*, 308, 1
- Mollá M., Vílchez J. M., Gavilán M., Díaz A. I., 2006, *MNRAS*, 372, 1069
- Mollá M., Cavichia O., Gavilán M., Gibson B. K., 2015, *MNRAS*, 451, 3693
- Neeleman M., Wolfe A. M., Prochaska J. X., Rafelski M., 2013, *ApJ*, 769, 54
- Nomoto K., Tominaga N., Umeda H., Kobayashi C., Maeda K., 2006, *Nucl. Phys. A*, 777, 424
- Oesch P. A. et al., 2014, *ApJ*, 786, 108
- Pagal B. E. J., Patchett B. E., 1975, *MNRAS*, 172, 13
- Peirani S. et al., 2017, *MNRAS*, 472, 2153
- Peng Y., Maiolino R., Cochrane R., 2015, *Nature*, 521, 192

- Pérez-Montero E. et al., 2016, *A&A*, 595, A62
 Petitjean P., Ledoux C., Srianand R., 2008, *A&A*, 480, 349
 Pettini M., Lipman K., Hunstead R. W., 1995, *ApJ*, 451, 100
 Pettini M., Ellison S. L., Bergeron J., Petitjean P., 2002, *A&A*, 391, 21
 Pilyugin L. S., 1993, *A&A*, 277, 42
 Pilyugin L. S., 1999, *A&A*, 346, 428
 Pilyugin L. S., Thuan T. X., Vílchez J. M., 2003, *A&A*, 397, 487
 Planck Collaboration XLVI et al., 2016a, *A&A*, 596, A107
 Planck Collaboration XLVII et al., 2016b, *A&A*, 596, A108
 Press W. H., Schechter P., 1974, *ApJ*, 187, 425
 Rollinde E., Vangioni E., Maurin D., Olive K. A., Daigne F., Silk J., Vincent F. H., 2009, *MNRAS*, 398, 1782
 Romano D., Karakas A. I., Tosi M., Matteucci F., 2010, *A&A*, 522, A32
 Schaerer D., 2002, *A&A*, 382, 28
 Scully S., Cassé M., Olive K. A., Vangioni-Flam E., 1997, *ApJ*, 476, 521
 Spite M. et al., 2005, *A&A*, 430, 655
 Springel V., Hernquist L., 2003, *MNRAS*, 339, 312
 Stanghellini L., Haywood M., 2010, *ApJ*, 714, 1096
 Stanghellini L., Guerrero M. A., Cunha K., Machado A., Villaver E., 2006, *ApJ*, 651, 898
 Talbot J. J. R., Arnett D. W., 1974, *ApJ*, 190, 605
 Taylor P., Kobayashi C., 2015, *MNRAS*, 452, L59
 Teyssier R., 2002, *A&A*, 385, 337
 Thuan T. X., Izotov Y. I., Lipovetsky V. A., 1995, *ApJ*, 445, 108
 Tinsley B. M., 1972, *A&A*, 20, 383
 Tinsley B. M., Larson R. B., 1978, *ApJ*, 221, 554
 Tissera P. B., Lambas D. G., Cora S. A., Mosconi M. B., 2002, *MNRAS*, 337, L27
 Tomkin J., Lambert D. L., 1984, *ApJ*, 279, 220
 Vader J. P., 1986, *ApJ*, 305, 669
 van den Hoek L. B., Groenewegen M. A. T., 1997, *A&AS*, 123, 305
 van Zee L., Haynes M. P., 2006, *ApJ*, 636, 214
 van Zee L., Salzer J. J., Haynes M. P., O'Donoghue A. A., Balonek T. J., 1998, *AJ*, 116, 2805
 Vangioni E., Olive K. A., Prestegard T., Silk J., Petitjean P., Mandic V., 2015, *MNRAS*, 447, 2575
 Vázquez G. A., Leitherer C., 2005, *ApJ*, 621, 695
 Ventura P., Stanghellini L., Dell'Agli F., García-Hernández D. A., 2017, *MNRAS*, 471, 4648
 Vincenzo F., Belfiore F., Maiolino R., Matteucci F., Ventura P., 2016, *MNRAS*, 458, 3466
 Woosley S. E., Weaver T. A., 1995, *ApJS*, 101, 181
 Wu Y.-Z., Zhang S.-N., 2013, *MNRAS*, 436, 934
 Zafar T., Centurión M., Péroux C., Molaro P., D'Odorico V., Vladilo G., Popping A., 2014, *MNRAS*, 444, 744

This paper has been typeset from a $\text{\TeX}/\text{\LaTeX}$ file prepared by the author.